



1 Improved maps of surface water bodies, large dams, reservoirs, and 2 lakes in China

3 Xinxin Wang^{1,2}, Xiangming Xiao^{2,*}, Yuanwei Qin², Jinwei Dong³, Jihua Wu⁴, Bo Li^{1,5,*}

4 ¹ Ministry of Education Key Laboratory for Biodiversity Science and Ecological Engineering,
5 National Observations and Research Station for Wetland Ecosystems of the Yangtze Estuary,
6 Institute of Biodiversity Science and Institute of Eco-Chongming, School of Life Sciences, Fudan
7 University, Shanghai 200438, China. ² Department of Microbiology and Plant Biology, Center for
8 Earth Observation and Modeling, University of Oklahoma, Norman, OK 73019, USA. ³ Key
9 Laboratory of Land Surface Pattern and Simulation, Institute of Geographic Sciences and Natural
10 Resources Research, Chinese Academy of Sciences, Beijing 100101, China. ⁴ State Key
11 Laboratory of Grassland Agro-Ecosystems, and College of Ecology, Lanzhou University, Lanzhou,
12 Gansu 730000, China. ⁵ Centre for Invasion Biology, Institute of Biodiversity, Yunnan University,
13 Kunming, Yunnan 650504, China

14 Corresponding authors: Xiangming Xiao, xiangming.xiao@ou.edu; Bo Li, bool@fudan.edu.cn

16 Abstract

17 Data and knowledge of surface water bodies (SWB), including large lakes and reservoirs
18 (surface water areas > 1 km²) are critical for the management and sustainability of water resources.
19 However, the existing global or national dam datasets have large georeferenced coordinate offsets
20 for many reservoirs, and some datasets have not reported reservoirs and lakes separately. In this
21 study, we generated China's surface water bodies, Large Dams, Reservoirs, and Lakes (China-
22 LDRL) dataset by analyzing all available Landsat imagery in 2019 (19,338 images) in Google
23 Earth Engine and very-high spatial resolution imagery in Google Earth Pro. There were ~3.52 ×
24 10⁶ yearlong SWB polygons in China for 2019, only 0.01 × 10⁶ of them (0.43%) were of large size
25 (> 1 km²). The areas of these large SWB polygons accounted for 83.54% of the total 214.92 × 10³



26 km² yearlong surface water area (SWA) in China. We identified 2,140 large dams, including 1,494
27 reservoir dams and 646 river dams, 1,976 large reservoirs (16.42×10^3 km²), and 3,508 large lakes
28 (75.97×10^3 km²). In general, most of the dams and reservoirs in China were distributed in South
29 China, East China, and Northeast China, whereas most of lakes were located in West China, the
30 Lower Yangtze River Basin, and Northeast China. The provision of the reliable, accurate China-
31 LDRL dataset on dams, large reservoirs and lakes will enhance our understanding of water
32 resources management and water security in China. The China-LDRL dataset is publicly available
33 at <https://doi.org/10.6084/m9.figshare.16964656.v2> (Wang et al., 2022).

34 1. Introduction

35 Surface water bodies (SWB), including large lakes and reservoirs (surface water areas > 1
36 km²), play an important role in the control and management of water resources (Yang and Lu, 2014,
37 2013; Feng et al., 2013, 2019). A reservoir is usually defined as artificial lake formed by
38 constructing dams across rivers (impoundment reservoir) (Thornton et al., 1996; Hayes et al., 2017)
39 or partially or completely formed by enclosed waterproof banks with concrete or clay (off-stream
40 reservoir) (Xiang et al., 2019; Thornton et al., 1996). Off-stream reservoirs usually include
41 mountain and plain reservoirs (**Fig. 1**). Nearly 50% of the global large dams were built primarily
42 for agricultural irrigation through storing, regulating, and diverting water (Mulligan et al., 2020).
43 Additionally, they are also used for hydropower generation, human and industrial uses, and flood
44 peak attenuation (Lehner et al., 2011; Lehner and Döll, 2004; Wang et al., 2021a). Large lakes
45 have been the subject of great interest not only because of their water resources but also as



46 indicators of local climate change and anthropogenic activities (Birkett and Mason, 1995; Ma et
47 al., 2011), and they could provide vital ecosystem services for human being, such as alteration of
48 river flow, supplies of irrigation water, fisheries, and abundant valuable mineral deposits, and have
49 disproportionate effects on the global carbon cycle (Ran et al., 2021; Armstrong, 2010; Ma et al.,
50 2011). Improved understanding of the detailed distributions of SWB, large dams, reservoirs, and
51 lakes could provide crucial information on water resources, environmental health, status of
52 ecosystems, and agricultural sustainability (Lehner and Döll, 2004).

53 **Insert Fig. 1 here**

54 China has the largest population, fastest-growing economy, increased expansion of irrigation,
55 relatively scarce water, dated infrastructure, and inadequate governance (Liu and Yang, 2012;
56 Wang et al., 2020a; Tao et al., 2020). China encompasses almost 20% of the world's population
57 but contains only 7% of the world's fresh water, and as the result, it has much smaller fresh water
58 resource per capital than do most other countries (Feng et al., 2019; Dalin et al., 2014). Since 1980s,
59 China has taken diverse measures to ensure the long-term water security (Zhou et al., 2020). For
60 example, China has a remarkable increase of reservoir construction across the country (Wang et
61 al., 2021a), and the total dam number increased to ~89,700 by 2008 in China (Yang and Lu, 2014).
62 The Three Gorges Reservoir, which is the world's largest hydroelectric dam (Three Gorges Dam),
63 is fully operational for flood control, power generation, navigation, and water use (Wu et al., 2004;
64 Zhang et al., 2012; Wang et al., 2013, 2020a). China also has a large number of lakes with
65 tremendously cultural and economic importance. Previous study reported that there were 2,693



66 large lakes (area > 1 km²) in China during 2005-2006, covering 0.9% of China's land area (Ma et
67 al., 2011). However, due to intensive human activities and climate change over the last three
68 decades, several natural lakes have converted into reservoirs, accelerating dramatically shrinkage
69 of lake areas (Yang and Lu, 2014; Ma et al., 2011). Therefore, the improved information on the
70 distribution of large reservoirs and lakes in China is needed for assessing the impact of human
71 activities and climate change on SWB, water management, and water security in China (Yang and
72 Lu, 2014).

73 There are several published global dam and reservoir datasets that include information from
74 China (**Table 1**). The World Register of Dams (WRD), which was published by the International
75 Commission on Large Dams (ICOLD, 2011), is the largest and widely-used dataset (Mulligan et
76 al., 2020; Paredes-Beltran et al., 2021; Wang et al., 2021a). It reports 23,841 dam entries for China,
77 however, a large proportion of those entries are not georeferenced with latitude and longitude
78 information, which limits its wide application (Wang et al., 2021a). The Global geOreferenced
79 Database of Dams (GOODD) V1 dataset reported 9,234 georeferenced dams in China (Mulligan
80 et al., 2020), however, the information (e.g. area, volume capacity) of all the corresponding
81 reservoirs was not reported. The FAO's (Food and Agriculture Organization of the United Nations)
82 global information system on water resources and agricultural water management (AQUASTAT)
83 lists 14,000 dams in the world, but only part of 722 dams in China were georeferenced, and has
84 not been updated since 2015. The Global Reservoir and Dam database (GRanD), developed by the
85 Global Water System Project (GWSP), compiled the available reservoir and dam information



86 globally (Lehner et al., 2011) and has been updated for the year 2019. However, it only lists 922
 87 geolocated dam entries for China. Recently, Wang et al. (2021a) released a global Georeferenced
 88 global dam and reservoir (GeoDAR) dataset with 5,347 georeferenced dams in China, and the
 89 reservoirs had more than 40 attributes acquired from the WRD dataset. However, our preliminary
 90 quality-check of the dataset shows that the georeference information of many dams in the GeoDAR
 91 dataset has moderate to substantial shifts (or offsets, mis-location), up to 500m or more (**Fig. S1**),
 92 indicating further improvement is needed before it can be used for geospatial analysis. There were
 93 also some published dam and reservoir maps at the national scale (**Table. 1**), but these maps neither
 94 included georeferenced dams nor reported reservoir attributes (e.g. reservoir area).

95 **Table 1. Information on published dam and reservoir datasets for the globe and China.**

Name	Spatial domain	Number of dams in the globe	Number of dams in China	Georeferenced dam?	Reservoir information (area ...)?
WRD	Global	~ 60000	23,841	Either not georeferenced or inaccessible.	Yes, > 40 attributes
GOODD V1	Global	38667	9,231	Yes	No
FAO AQUASTAT	Global	14000	722	Partly georeferenced	Yes, reservoir capacity and area
GRanD	Global	7320	922	Yes	Yes, ~ 50 attributes
GeoDAR	Global	23680	5,345	Yes	Yes, attributes from WRD dataset
CLRM	China	/	89,700	No	Yes, reservoir capacity and area
BFNCW	China	/	98,002	No	No

96 WRD: the World Register of Dams (<https://www.icold-cigb.org>); GOODD: GLObal geOreferenced Database of
 97 Dams (Mulligan et al., 2020); FAO AQUASTAT: The Food and Agriculture Organization of the United Nations



98 (FAO) global information system on water resources and agricultural water management
99 (<http://www.fao.org/aquastat/en/databases/dams/>); GRanD: the Global Reservoir and Dam database (Lehner et
100 al., 2011); GeoDAR: Georeferenced global dam and reservoir dataset (Wang et al., 2021a); CLRM: China's
101 Lakes and Reservoirs Map (Yang and Lu, 2014); BFNCW: Bulletin of First National Census for Water from
102 Ministry of Water Resources the People's Republic of China (<http://www.mwr.gov.cn/2013pcgb/index.html>). “/”
103 means these data were published in China, but global dam information is unavailable.

104

105 In addition to the dam and reservoir datasets, several studies have reported the spatial
106 distribution and multi-year dynamics of inland SWB (Tao et al., 2020; Ma et al., 2011; Wang et
107 al., 2020a; Feng et al., 2019) and lakes (Gao, 2015; Gao et al., 2012; Yang and Lu, 2014; Ma et al.,
108 2011) in China, however, they did not explicitly explore the spatial distribution of large reservoirs
109 and lakes in China, making it impossible to assess the impact of human activities on these two
110 types of water resources (Yang and Lu, 2014). Thus, to date, the spatial distributions of SWB, large
111 dams, reservoirs, and lakes in China have not been fully investigated and documented, yet.

112 The objective of this study was to produce detailed and accurate maps of open SWB, large
113 dams, reservoirs, and lakes (surface water area > 1 km²) in China in 2019, the latest year when this
114 study started in late 2020. First, this study used time-series Landsat imagery in 2019 and Google
115 Earth Engine (GEE) cloud computing platform as well as the simple and robust surface water
116 mapping algorithm (Zou et al., 2018, 2017; Zhou et al., 2019b; Wang et al., 2020a) to generate
117 raster maps of SWB in China at 30-m spatial resolution. Second, we converted the raster map of



118 SWB to a vector map of SWB and identified those large SWB with area $> 1 \text{ km}^2$. Third, we
119 combined the vector map of SWB with the historical satellite images in 2019 within China in
120 Google Earth Pro to identify dams and released China's surface water bodies, large dams,
121 reservoirs, and lakes dataset, namely, China-LDRL. Forth, we analyzed the spatial distribution of
122 SWB, large dams, reservoirs, and lakes in China. Finally, we discussed the reliabilities,
123 uncertainties, limitations, outlooks, and implications of the China-LDRL dataset.

124

125 **2. Materials and Methods**

126 **2.1 Study area**

127 The study area covered all the provincial-level administrative divisions in China (**Fig. 2a**),
128 including 23 provinces, 2 special administrative regions (Hong Kong and Macao), 4 municipalities
129 (Beijing, Tianjin, Shanghai, and Chongqing), and 5 Autonomous Regions (Inner Mongolia,
130 Guangxi, Tibet, Ningxia, and Xinjiang). Since Macao and Hong Kong have relatively small areas
131 and are very close to Guangdong Province, we combined them as one region (Guangdong) when
132 we performed the statistical analysis in this study.

133 **2.2 Data**

134 **2.2.1 Landsat data**

135 In this study, we used the available Landsat surface reflectance (SR) images in the GEE



136 platform, and there was a total of 19,338 images in 2019 for China, including 9,028 Landsat-7
137 ETM+ images and 10,310 Landsat-8 OLI images (~21.73 TB). The detailed information of
138 Landsat SR products is available on the GEE platform ([https://developers.google.com/earth-](https://developers.google.com/earth-engine/datasets/catalog/landsat)
139 [engine/datasets/catalog/landsat](https://developers.google.com/earth-engine/datasets/catalog/landsat), last access: 18 February 2022). All these images had undergone
140 necessary pre-processing in GEE, including radiometric calibration and atmospheric correction.
141 We used the quality assurance (QA) band that was generated by the CFMASK algorithm (Zhu et
142 al., 2015) to identify bad-quality observations, including clouds and cloud shadows (Murray et al.,
143 2019; Pekel et al., 2016). We also used the Shuttle Radar Topography Mission (SRTM) digital
144 elevation model (DEM) data, the solar azimuth and zenith angle data of each image, and
145 ee.Terrain.hillShadow algorithm in GEE to identify those pixels with terrain shadows (Zou et al.,
146 2018; Wang et al., 2020a) (**Fig. 2b**), which were excluded from the data analysis. Out of ~132.43
147 million pixels in China, approximately 98.36% had more than 5 good-quality observations and
148 91.24% had more than 10 good-quality observations in 2019. About 93.14% of the 78.9 million
149 pixels in North China had more than 20 good-quality observations due to the overlapping of
150 Landsat images at the high latitudes and less cloud cover (Zhou et al., 2019a; Wang et al., 2020b).
151 Note that number of Landsat-7 ETM+ images in GEE may change in the future, as USGS continues
152 to work with the International Ground stations (IGS) in the world to assemble and rescue some
153 images from individual stations. For Landsat-8 OLI images, USGS does not rely on IGS for image
154 downlink, as its data record is able to store all the images and then downlink them to the Landsat
155 archive (Wulder et al., 2016).



156 We used three spectral indices (NDVI, EVI, mNDWI) to identify SWB in this study. These

157 indices are defined as:

$$158 \quad NDVI = \frac{\rho_{nir} - \rho_{red}}{\rho_{nir} + \rho_{red}} \quad (1)$$

$$159 \quad EVI = 2.5 \times \frac{\rho_{nir} - \rho_{red}}{\rho_{nir} + 6 \times \rho_{red} - 7.5 \times \rho_{blue} + 1} \quad (2)$$

$$160 \quad mNDWI = \frac{\rho_{green} - \rho_{swir}}{\rho_{green} + \rho_{swir}} \quad (3)$$

161 where ρ_{blue} , ρ_{green} , ρ_{red} , ρ_{nir} , and ρ_{swir} are blue, green, red, near-infrared, and shortwave
162 infrared bands of Landsat images.

163 **Insert Fig. 2 here**

164 **2.2.2 Dam and reservoir datasets**

165 The Global GeOreferenced Database of Dams (GOODD) dataset was released in 2020 and it
166 lists ~38,000 georeferenced dams as well as derived data on their associated catchments through
167 one by one degree titles on the Google Earth geobrowser during 2007-2011 and the Shuttle Radar
168 Topography Mission (SRTM) Water Body Dataset (SWBD) (Mulligan et al., 2020). It provides the
169 raw digitized coordinates for the locations of dam walls, but it does not provide the detailed
170 attribute data on the characteristics of each dam and reservoir (**Fig. 3a, d**). Both the large dams
171 and medium sized dams were captured in this dataset.

172 The Global Reservoir and Dam (GRanD) Database v1.3 was recently updated in February
173 2019 by Lehner et al. (2011) (**Fig. 3b, e**). The spatial information of these dams was contributed
174 by eleven participating institutions. Each dam was assigned to a polygon that depicted the reservoir



175 surface, which was provided by SWBD (v1.1) and the surface water maps produced by the Joint
176 Research Center (JRC) of the European Commission from Landsat imagery at 30-m spatial
177 resolution for the period 1984-2015 (Pekel et al., 2016) (v1.3). All reservoirs with a storage
178 capacity of more than 0.1 km³ were included in this dataset, and some smaller reservoirs were also
179 added when their data were available.

180 The Georeferenced global Dam And Reservoir dataset (GeoDAR) was produced by utilizing
181 multi-source dam and reservoir inventories (ICOLD WRD and GRanD v1.3 datasets) and the
182 Google Maps geocoding API (Wang et al., 2021a) (**Fig. 3d, e**). The GeoDAR product includes two
183 successive versions. GeoDAR v1.0 is essentially a georeferenced subset of ICOLD WRD, and
184 contains more than 20,000 dam entries, and each of which is indexed by an encrypted identifier
185 (ID) that is associated with a WRD record, allowing for the potential retrieval of all its 40+
186 proprietary attributes from ICOLD. GeoDAR v1.1 consists of (1) dam entries as in v1.0 except
187 those that further harmonized with GRanD for an improved inclusion of the largest dams, and (2)
188 reservoir boundaries for most of the dam entries.

189 **Insert Fig. 3 here**

190 **2.3 Methods**

191 The workflow for producing the China-LDRL dataset included major two sections: 1)
192 generation of yearlong SWB maps in China by analyzing time-series Landsat imagery in 2019
193 with GEE platform, and 2) identification of dams and classification of yearlong SWB into lakes,



194 reservoirs, and rivers by analyzing the historical satellite images in 2019 within China in Google
195 Earth Pro. A flowchart showing the methodology of this study is illustrated in **Fig. 4**.

196 **Insert Fig. 4 here**

197 **2.3.1 Algorithm to generate annual map of yearlong surface water bodies**

198 In this study, we combined a surface water index (mNDWI) and two greenness-based
199 vegetation indices (EVI and NDVI) to identify SWB through the algorithm of ((mNDWI > EVI or
200 mNDWI > NDVI) and EVI < 0.1) (Eq. (4)). This mNDWI/VIs algorithm can reduce the effects of
201 vegetation on identification of SWB, and was widely used to identify and map SWB at the regional
202 and national scales with high accuracy (Zou et al., 2018, 2017; Zhou et al., 2019b; Wang et al.,
203 2020a). Furthermore, this mNDWI/VIs algorithm had been compared with other surface water
204 body mapping algorithms (e.g. NDWI, mNDWI, TCW, and AWEI), and the results showed that
205 this algorithm and Landsat images could identify SWB with high producer's accuracy (98.1%)
206 and user's accuracy (91.0%) (Zhou et al., 2017).

207 Surface water body frequency (F_{SWB}) of a pixel was calculated as the ratio of the number of
208 observations identified as surface water body to the number of good-quality observations in a year
209 and scaled from 0 to 1.0 (or 100%) (Zou et al., 2017), see Eq. (5). We generated the F_{SWB} map
210 of all the pixels in China for 2019 in the GEE platform (**Fig. 5a**).

$$211 \quad SWB = \begin{cases} 1, & (\text{mNDWI} > \text{EVI} \text{ or } \text{mNDWI} > \text{NDVI}) \text{ and } \text{EVI} < 0.1 \\ 0, & \text{Other values} \end{cases} \quad (4)$$

$$212 \quad F_{SWB} = \frac{N_{SWB}}{N_{good}} \quad (5)$$



213 where SWB is surface water body, F_{SWB} is surface water body frequency, N_{SWB} is the number
214 of observations identified as SWB (see Eq. (4)) in 2019, N_{good} is the number of good-quality
215 observations in 2019.

216 Consistent with our previous publications (Zou et al., 2018; Wang et al., 2020a), a water pixel
217 was defined as yearlong surface water ($F_{SWB} \geq 0.75$), seasonal surface water ($0.05 \leq F_{SWB} <$
218 0.75), or ephemeral surface water ($F_{SWB} < 0.05$). We generated the seasonal and yearlong SWB
219 maps in China for 2019, respectively (**Fig. 5b, c**).

220 **Insert Fig. 5 here**

221 **2.3.2 The procedure to identify dams, reservoirs, and lakes in Google Earth Pro**

222 We first generated the yearlong SWB vector map in China for 2019 based on the yearlong
223 SWB raster map, then reprojected it to the Krasovsky_1940_Albers equal-area conic projection
224 and calculated the area of each yearlong SWB polygon within China (Python code is available in:
225 <https://drive.google.com/drive/folders/1B19VKbCIoDPmu-IcmiZcOIUF8wi1YnE?usp=sharing>).
226 When we reported large reservoirs and lakes, only polygon with area $> 1 \text{ km}^2$ was kept in this
227 study. In an effort to distinguish riverine or off-channel reservoirs from lakes, we uploaded the
228 large SWB vector layer into Google Earth Pro, and checked whether a dam existed around each
229 polygon through the historical satellite images in 2019 within China by visual image interpretation
230 approach. If a dam did not exist, we classified the polygon as river or lake; if a dam did exist, the
231 polygon would be classified as impoundment reservoir or off-stream reservoir. Simultaneously, we



232 classified the corresponding dams as river dams or reservoir dams. Finally, the SWB polygons
233 were classified into lakes, reservoirs, and rivers, and the dams were classified into reservoir dams
234 and river dams (**Fig. 4**). This work was carried out and completed by the lead author (Dr. Wang)
235 over one month, and users could reproduce the dam dataset by uploading the SWB polygons in
236 the historical satellite images in 2019 in Google Earth Pro and following the procedure described
237 here. Note that satellite images in the Google Earth Pro may change over time, but such change
238 may have very limited impact on identification of dam as dam often exists over many years after
239 its construction.

240 **2.4 Calculation of lake and reservoir attributes**

241 The areas (km²) of SWB polygons were generated using the Krasovsky_1940_Albers
242 coordinate system. As we generated the vector maps of yearlong and seasonal SWB in China for
243 2019, we calculated the yearlong SWB areas linked to the dams as the reservoir areas. Likewise,
244 we also calculated each lake area as its attribute in our study.

245 **2.5 Cross-comparison with other lake and reservoir datasets**

246 To better understand the improvements and potential application of our China-LDRL dataset,
247 we compared it with other three available dam and reservoir datasets: the GOODD, GRanD V1.3,
248 and GeoDAR datasets (**Fig. 3**). We first compared the dam quantity and areas of large reservoir at
249 the provincial and national scales. Then, we checked the spatial distribution of each dam from
250 these datasets within Google Earth imagery as all these datasets provide detailed georeferenced



251 coordinates for some of dams, and the georeferenced information could be directly acquirable from
252 the spatial longitude and latitude. Here we did not compare the reservoir area with the GOODD
253 dataset as it does not provide such attribute except catchment area (**Fig. 3d**).

254 **3. Results**

255 **3.1 Annual map of surface water bodies in China for 2019**

256 Surface water body frequency (F_{SWB}) of individual pixels for 2019 varied substantially across
257 China (**Fig. 5**). There were ~ 3.38 million seasonal surface water pixels (30-m spatial resolution)
258 in China, amounting to $\sim 3,375.88 \times 10^3$ km² seasonal surface water area (SWA) in 2019. Xinjiang
259 Province had the largest seasonal SWA (751.14×10^3 km²), followed by Tibet (600.70×10^3 km²),
260 Qinghai (564.57×10^3 km²), Inner Mongolia (511.42×10^3 km²), and Heilongjiang Province
261 (343.33×10^3 km²) (**Fig. 6a**). There were ~ 0.21 million yearlong surface water pixels in China for
262 2019, amounting to $\sim 214.92 \times 10^3$ km² yearlong SWA, which were mainly located in Tibet (62.65
263 $\times 10^3$ km²), Qinghai (41.08×10^3 km²), and Xinjiang (24.60×10^3 km²) Provinces (**Fig. 6b**).
264 Additionally, Heilongjiang, Jiangsu, Inner Mongolia, Hubei, and Anhui Provinces also had relative
265 larger yearlong SWA ($> 5 \times 10^3$ km²) than other provinces in China.

266 **Insert Fig. 6 here**

267 **3.2 Numbers and areas of yearlong surface water bodies with different sizes in China**

268 The numbers and areas of yearlong SWB polygons of different sizes in China differed
269 considerably for 2019 (**Fig. 7**). In terms of yearlong SWB numbers, out of a total of 3.52×10^6



270 yearlong SWB polygons in China in 2019, approximate 3.51×10^6 polygons (99.57%) had an area
271 of $\leq 1 \text{ km}^2$, and $\sim 2.16 \times 10^6$ polygons (61.19%) had an area of $\leq 0.0036 \text{ km}^2$ (covering only 2×2
272 Landsat grid cells). Only 15×10^3 (0.43%) yearlong SWB polygons had an area of $> 1 \text{ km}^2$, and
273 359 polygons had an area of $> 100 \text{ km}^2$. In terms of yearlong SWB areas, out of a total of 214.92
274 $\times 10^3 \text{ km}^2$ yearlong SWA in China in 2019, large SWB polygons (size $> 1 \text{ km}^2$) accounted for
275 83.54%, and very large SWB polygons (size $> 100 \text{ km}^2$) accounted for 52.48%.

276 The numbers and areas of yearlong SWB polygons of different sizes at the provincial scale
277 had similar distribution patterns with those at the national scale (**Fig. S2, S3**). Almost all the
278 yearlong SWB polygons in individual provinces had an area of $\leq 1 \text{ km}^2$ (**Fig. S2**), however, those
279 SWB polygons with an area of $> 1 \text{ km}^2$ accounted for a large proportion of SWA in most provinces
280 (**Fig. S3**). Those yearlong SWB polygons with an area of $> 100 \text{ km}^2$ were mostly very large lakes
281 and rivers, and they were mainly located in Tibet, Xinjiang, Qinghai, Jiangxi, and Heilongjiang
282 Provinces (**Fig. S3**) (Feng et al., 2019). Some provinces also had very large-size reservoirs, such
283 as Miyun Reservoir in Beijing, whose polygon size was greater than 100 km^2 .

284 **Insert Fig. 7 here**

285 **3.3 Numbers, areas, and distribution of large dams, reservoirs, and lakes in China**

286 We identified 2,140 large dams in China, including 1,494 reservoir dams and 646 river dams,
287 most of which were located in South, East, and Northeast China, as well as Tianshan Mountains
288 in Xinjiang of Northwest China (**Fig. 8a**). At the provincial scale, Heilongjiang Province had the



289 largest number of reservoir dams (148), followed by Shandong (147), Hubei (143), Guangdong
290 (122), and Jilin (121) Provinces. There were also five provinces (Xinjiang, Yunnan, Liaoning,
291 Henan, and Anhui) had relatively larger reservoir dam numbers (> 50) than other provinces.
292 Shanghai (1), Tibet (1), and Qinghai Province (2) had very small numbers of reservoir dams (< 5)
293 (**Fig. 8b**). Most of river dams in China were distributed in those provinces with large rivers.
294 Guangdong had the largest number of river dams (90) in China, followed by Sichuan (84), Hunan
295 (58), Fujian (43), and Yunnan Province (40). However, there were no river dams in Jiangsu and
296 Shanghai (**Fig. 8c**). In terms of the functions of two kinds of dams and the spatial patterns of
297 climate (e.g. precipitation, temperature) and social-economic factors (e.g. population, GDP,
298 irrigation area) in South and North China, the provinces in Northeast and East China had larger
299 percentage of reservoir dams, whereas the provinces in South and Southwest China had larger
300 percentage of river dams (**Fig. 8d**).

301 **Insert Fig. 8 here**

302 China had 3,508 large lakes with an area of $> 1 \text{ km}^2$ in 2019, most of which were distributed
303 in West China, the Lower Yangtze River Basin, and Northeast China (**Fig. 9a, S4**), and they
304 together amounted to $\sim 75.97 \times 10^3 \text{ km}^2$. Tibet in West China had the largest lake number (978),
305 followed by Qinghai (482), Xinjiang (388), Inner Mongolia (241), and Hubei Province (218) (**Fig.**
306 **9b**). The lake areas in China had similar spatial patterns with the lake numbers (**Fig. 9c**), and the
307 western provinces in China had much larger lake areas than other provinces, especially Tibet and
308 Qinghai Provinces with $32.51 \times 10^3 \text{ km}^2$ and $16.47 \times 10^3 \text{ km}^2$, respectively. As reservoirs and dams



309 usually exist simultaneously, the spatial patterns of reservoir numbers and areas matched well with
310 those of dam numbers (**Figs. 8b, 9e-f**). In total, China had 1,976 large reservoirs in 2019, they
311 together amounted to an area of $\sim 16.42 \times 10^3$ km². Hubei Province in Northeast China had the
312 largest reservoir area (2177.96 km²), followed by Jilin (1,323.29 km²), Heilongjiang (1,320.40
313 km²), and Henan Province (1304.60 km²). In contrast, Tibet (18.34 km²), Shanghai (36.14 km²),
314 and Taiwan Province (54.89 km²) had much smaller reservoir areas than other provinces in China.
315 In general, most of the dams and reservoirs in China were distributed in South China, East China,
316 and Northeast China, whereas most of lakes were located in West China, the Lower Yangtze River
317 Basin, and Northeast China (**Figs. 8, 9**).

318 **Insert Fig. 9 here**

319 **4. Discussion**

320 **4.1 Improvements of the dataset of large dams, reservoirs, and lakes in China**

321 In order to validate the reliability of our China-LDRL dataset, we first compared the numbers
322 of large dams and areas of large reservoirs between our dataset and published datasets (GOODD,
323 GRanD, and GeoDAR), then we checked the geographical coordinates of dams within the
324 historical satellite images in 2019 in Google Earth Pro.

325 The GOODD dataset has the largest number of dams (9,231) in China among these published
326 global datasets (**Fig. 10a**). However, it includes both large, moderate, and small dams, and does
327 not report the corresponding reservoir attributes (e.g. reservoir area), which limits its applications



328 to water-related research (Paredes-Beltran et al., 2021). The GRanD dataset has the smallest
329 number (814) of large dams with reservoir area $> 1 \text{ km}^2$ in China (**Fig. 10b, e**) as the dam
330 information was provided by multiple institutions from the world (Lehner et al., 2011), which
331 clearly underestimates the number of dams. The GeoDAR dataset has a larger number of large
332 dams (993) than the GRanD dataset, because it was generated by combining the GRanD and
333 ICOLD WRD datasets (Wang et al., 2021a). However, our China-LDRL dataset identified 2,140
334 large dams and 1,976 large reservoirs (**Fig. 10d, e, f**), making substantial improvement of large
335 dam and reservoir dataset in China. The number differences of large dams between our China-
336 LDRL and the GRanD and GeoDAR datasets could be explained by several factors. First, our
337 study used all the available Landsat images in 2019 and accurate SWB mapping algorithm to
338 generate SWB maps in China, however, the GRanD and GeoDAR datasets used the SWBD map
339 (produced in 2000) (Slater et al., 2006) and the surface water maps during 1984-2015 produced by
340 the JRC (Pekel et al., 2016), thus, we could integrate more Landsat images and get more SWB
341 polygons, as well as larger numbers of large dams and reservoirs than other datasets. In addition,
342 the different strategies for identifying dams also caused the differences of dam numbers. The dam
343 information from the GRanD dataset was contributed by eleven participating institutions, and the
344 GeoDAR dataset combined two published dam datasets (WRD and GRanD) and rechecked
345 detailed dam information, then reported the georeferenced information. Unlike the GRanD and
346 GeoDAR datasets, our study first generated SWB raster and vector maps using the mNDWI/VIs
347 SWB mapping algorithm, and then selected the large yearlong SWB polygons with area $> 1 \text{ km}^2$.
348 After that, we visually checked the large SWB polygons one by one and identified each dam with



349 accurate geographical coordinates.

350 **Insert Fig. 10 here**

351 In addition to the dam numbers, we also compared the reservoir areas between different
352 datasets (**Fig. 11**). Our China-LDRL dataset reports $\sim 16.42 \times 10^3$ km² large reservoir area, which
353 was smaller than those of the GRanD (20.98×10^3 km²) and GeoDAR (21.84×10^3 km²) datasets.
354 We checked the reservoir polygons of the three datasets in Google Earth Pro, and found that some
355 large lakes were identified as reservoirs by the GranD and GeoDAR datasets, such as the Hongze
356 Lake in Jiangsu Province (**Fig. S5a**), contributing to the overestimate of reservoir areas. In addition,
357 the GRanD v1.3 dataset linked the “maximum surface water extent” from the JRC dataset to the
358 corresponding dams as the reservoir regions, however, we used the “yearlong surface water body”
359 to depict the reservoir in the China-LDRL dataset, which caused our smaller reservoir areas (**Fig.**
360 **S5b-e**).

361 **Insert Fig. 11 here**

362 In this study, we also checked the accuracy of geographical coordinates of dams from these
363 dam datasets. Here we first uploaded above-mentioned three dam datasets and our China-LDRL
364 dataset in the Google Earth Pro and visually checked the spatial distribution of each dam within
365 the historical satellite images in 2019 (**Fig. 12**). We found that the dam locations of the GOODD
366 dataset had substantial geographic offsets, some of which are larger than 500 m (**Fig. S6**). We
367 further overlapped the GOODD dam layer with our yearlong SWB map (Section 2.3.1), and the



368 results showed that only $12.52 \pm 3.87\%$ of the GOODD dams were intersected with the SWB layer
369 at the national scale (**Fig. 13a**). In the case that we applied a 100-m and 500-m tolerance when
370 intersecting the GOODD dams with our yearlong SWB map for 2019, the intersection rate
371 increased to only $47.58 \pm 9.70\%$ and $76.46 \pm 7.11\%$, respectively (**Figs. 13b, S7**). In addition, we
372 applied different tolerances when intersecting the GRanD and GeoDAR datasets with our yearlong
373 SWB layer. About $65.57 \pm 6.79\%$ of the dams in the GRanD dataset were intersected with our
374 yearlong SWB map (**Fig. 13a**), which increased to $87.52 \pm 6.45\%$ and $95.94 \pm 4.49\%$ when using
375 a 100-m and 500-m tolerance (**Figs. 13b, S7**). Although the GeoDAR dataset is released by
376 integrating the GRanD dataset, its geographical coordinates also had larger offsets (**Fig. 12d, f, g**),
377 and $41.10 \pm 6.13\%$ of its dams were intersected with the yearlong SWB layer, and $63.18 \pm 5.61\%$
378 and $86.69 \pm 3.74\%$ intersected when the tolerance was 100-m and 500-m (**Figs. 13b, S7**). These
379 comparisons suggested the substantial geographic offsets of these published datasets (GOODD,
380 GRanD, and GeoDAR), and improved accuracy of our China-LDRL dataset, which could provide
381 important and reliable information for water resource management and water security in China.

382 **Insert Fig. 12 here**

383 **Insert Fig. 13 here**

384 **4.2 Uncertainties, limitations, outlooks, and implications**

385 In this study, we produced detailed and accurate China's open surface water bodies, large
386 dams, reservoirs, and lakes (China-LDRL) dataset for 2019, and analyzed their spatial distribution



387 patterns. This study benefited from the usage of time-series Landsat imagery and GEE cloud
388 computing platform, as well as simple and robust SWB mapping algorithms. First, time series
389 Landsat images at high spatial resolution (30-m) provide larger numbers of good-quality
390 observations for identifying SWB. Second, GEE cloud computing platform enables us to acquire
391 and analyze tens of thousands of Landsat images in hours. Third, the mNDWI/VIs algorithm used
392 in this study could reduce the uncertainties induced by the bad-quality observations and provide
393 accurate SWB maps. Finally, we visually checked the large SWB polygons (area > 1 km²) one by
394 one by using the historical satellite images in 2019 within China in Google Earth Pro, and we
395 recorded the georeferenced coordinates of individual dams in China for 2019.

396 We would also acknowledge that the data quality of input satellite images remains to be a
397 concern for the identification of dams, reservoirs, and lakes. The spatial distribution of good-
398 quality observations of Landsat data shows that more than 98.36% of the total 30-m pixels in China
399 had more than 5 good-quality observations and more than 91.24% of the total pixels had more than
400 10 good-quality observations for 2019 (**Fig. 2b**), but the regions with complex topography and
401 mountains, such as South and Southwest China, had much fewer good-quality observations than
402 other regions, which might underestimate surface water areas, as well as dam and reservoir
403 numbers and areas. In addition, it is impossible to remove all the bad-quality observations (e.g.
404 clouds, terrain shadows) because of the limited quality of the QA band and digital elevation model
405 data in GEE. Therefore, the remaining bad-quality observations could result in some inevitable
406 uncertainties in the resultant maps. In the future, as more images from Landsat dataset and other



407 high spatial resolution sensors (e.g., Sentinel-1, Sentinel-2) are added into GEE platform (Wulder
408 et al., 2016), SWB mapping accuracy could be further improved, providing more detailed
409 geospatial data of dams, reservoirs, and lakes in China.

410 In our China-LDRL dataset, we identified and reported those large SWB, however, the
411 importance of monitoring small water bodies (area ≤ 1 km²) and dams is gradually recognized as
412 they play critical roles in accurate assessments of their agricultural potential or their cumulative
413 influence in watershed hydrology (Ogilvie et al., 2018). In the near future, we can include these
414 small SWB polygons into our dataset to enhance the spatial details and distributions of dams,
415 reservoirs, and lakes in China.

416 The conversions between rivers, lakes, and reservoirs have critical effects on the ecosystem
417 services. For example, the construction of the Three Gorges Dam contributed to the decrease of
418 surface water area and biodiversity in its downstream areas (Fang et al., 2006; Feng et al., 2013;
419 Wang et al., 2020a), and reduced the sediment loads in the Yangtze River, causing the decreased
420 deposition rates of coastal wetlands in the Yangtze Delta (Feng et al., 2016; Wang et al., 2021b).
421 Furthermore, the conversion from natural lakes and rivers to man-made reservoirs has
422 disproportionate effects on the local, regional, and global carbon cycle (Howard Coker et al., 2009).
423 For example, dam construction has reduced the areal extent of CO₂ gas exchange in natural rivers
424 (Ran et al., 2021). In the future, more detailed information (e.g. construction year of dam) could
425 be included in our China-LDRL dataset, making it possible to analyze the effects of conversions
426 from natural lakes and rivers to reservoirs on the biodiversity and carbon cycle.



427

428 **5. Data availability**

429 The China-LDRL dataset is publicly available at
430 <https://doi.org/10.6084/m9.figshare.16964656.v2> (Wang et al., 2022), and it includes three
431 shapefiles. The “China_large_dams_attribute.shp” is the large dams in China, as well as their
432 attributes (including ID, dam class, longitude and latitude, polygon area, and corresponding
433 reservoir ID). The “China_large_lakes.shp” and “China_large_reservoirs.shp” are the large lakes
434 and reservoir maps in China.

435 **6. Code availability**

436 Code used in calculations of surface water bodies is available upon request. Code for transferring
437 the images to vector maps in Python could be found in:
438 <https://drive.google.com/drive/folders/1B19VKbCIoDPmu-IcmiZcOIUF8wi1YnE?usp=sharing>.

439

440 **7. Conclusion**

441 Several studies have published global or national dam, reservoir, and lake datasets based on
442 satellite images (**Table 1**). However, these datasets usually have large georeferenced coordinate
443 offsets, which poses some limitations to those studies that aim to address major issues in hydrology,
444 ecology, and water resource management in China. In this study, we generated the dataset of



445 China's open surface water bodies, large dams, reservoirs, and lakes (China-LDRL) for 2019, and
446 then analyzed their spatial distributions at the provincial and national scales. Satellite image data
447 quality is still a major source of uncertainty that affects the accuracy of the surface water body
448 maps. As more images from Landsat datasets and other high spatial resolution sensors (e.g.,
449 Sentinel-1, Sentinel-2) are added into GEE platform, the accuracy of SWB maps can be further
450 improved, providing more detailed geospatial data of dams, reservoir, and lakes in China. The
451 provision of the reliable, accurate China-LDRL dataset on dams, reservoirs, and lakes will
452 contribute to the understanding of water crisis and water resources management in China.

453 **Author contribution**

454 X.X., X.W., and B.L. designed the study. X.W. carried out image data processing and led
455 interpretation of the results and writing of the manuscript. Y.Q., and J.D. contributed to image data
456 processing, X.X., B.L., Y.Q., J.D., and J. W. contributed to the interpretation and discussion of the
457 results.

458 **Declaration of Competing Interest**

459 The authors declare that they have no known competing financial interests or personal
460 relationships that could have appeared to influence the work reported in this paper.

461 **Acknowledgements**

462 This study was supported in part by research grants from the U.S. National Science Foundation
463 (1911955), the Natural Science Foundation of China (81961128002), the China Postdoctoral



464 Science Foundation (2021M700835 and 2021TQ0072), and the China Scholarship Council
465 (201906100124).

466 **References**

467 Armstrong, A.: Lake carbon, *Nat. Geosci.*, 3, 151, <https://doi.org/10.1038/ngeo816>, 2010.

468 Birkett, C. M. and Mason, I. M.: A New Global Lakes Database for a Remote Sensing Program

469 Studying Climatically Sensitive Large Lakes, *J. Great Lakes Res.*, 21,

470 [https://doi.org/10.1016/S0380-1330\(95\)71041-3](https://doi.org/10.1016/S0380-1330(95)71041-3), 1995.

471 Dalin, C., Hanasaki, N., Qiu, H., Mauzerall, D. L., and Rodriguez-Iturbe, I.: Water resources

472 transfers through Chinese interprovincial and foreign food trade, *Proc. Natl. Acad. Sci. U. S. A.*,

473 111, 9774–9779, <https://doi.org/10.1073/pnas.1404749111>, 2014.

474 Fang, J., Wang, Z., Zhao, S., Li, Y., Tang, Z., Yu, D., Ni, L., Liu, H., Xie, P., Da, L., Li, Z., and

475 Zheng, C.: Biodiversity changes in the lakes of the Central Yangtze,

476 [https://doi.org/10.1890/1540-9295\(2006\)004\[0369:BCITLO\]2.0.CO;2](https://doi.org/10.1890/1540-9295(2006)004[0369:BCITLO]2.0.CO;2), 2006.

477 Feng, L., Hu, C., Chen, X., and Zhao, X.: Dramatic inundation changes of China's two largest

478 freshwater lakes linked to the Three Gorges Dam, *Environ. Sci. Technol.*, 47, 9628–9634,

479 <https://doi.org/10.1021/es4009618>, 2013.

480 Feng, L., Han, X., Hu, C., and Chen, X.: Four decades of wetland changes of the largest

481 freshwater lake in China: Possible linkage to the Three Gorges Dam?, *Remote Sens. Environ.*,



- 482 176, 43–55, <https://doi.org/10.1016/j.rse.2016.01.011>, 2016.
- 483 Feng, S., Liu, S., Huang, Z., Jing, L., Zhao, M., Peng, X., Yan, W., Wu, Y., Lv, Y., Smith, A. R.,
484 McDonald, M. A., Patil, S. D., Sarkissian, A. J., Shi, Z., Xia, J., and Ogbodo, U. S.: Inland water
485 bodies in China: Features discovered in the long-term satellite data, *Proc. Natl. Acad. Sci. U. S.*
486 *A.*, 116, 25491–25496, <https://doi.org/10.1073/pnas.1910872116>, 2019.
- 487 Gao, H.: Satellite remote sensing of large lakes and reservoirs: from elevation and area to
488 storage, *Wiley Interdiscip. Rev. Water*, 2, 147–157, <https://doi.org/10.1002/wat2.1065>, 2015.
- 489 Gao, H., Birkett, C., and Lettenmaier, D. P.: Global monitoring of large reservoir storage from
490 satellite remote sensing, *Water Resour. Res.*, 48, W09504,
491 <https://doi.org/10.1029/2012WR012063>, 2012.
- 492 Hayes, N. M., Deemer, B. R., Corman, J. R., Razavi, N. R., and Strock, K. E.: Key differences
493 between lakes and reservoirs modify climate signals: A case for a new conceptual model,
494 *Limnol. Oceanogr. Lett.*, 2, 47–62, <https://doi.org/10.1002/lol2.10036>, 2017.
- 495 Howard Coker, E., Hotchkiss, R. H., and Johnson, D. A.: Conversion of a Missouri River Dam
496 and Reservoir to a Sustainable System: Sediment Management¹, *JAWRA J. Am. Water Resour.*
497 *Assoc.*, 45, 815–827, <https://doi.org/10.1111/j.1752-1688.2009.00324.x>, 2009.
- 498 ICOLD: World register of dams, Paris, 2011.
- 499 Lehner, B. and Döll, P.: Development and validation of a global database of lakes, reservoirs and



- 500 wetlands, *J. Hydrol.*, 296, 1–22, <https://doi.org/10.1016/j.jhydrol.2004.03.028>, 2004.
- 501 Lehner, B., Liermann, C. R., Revenga, C., Vörösmarty, C., Fekete, B., Crouzet, P., Döll, P.,
502 Endejan, M., Frenken, K., Magome, J., Nilsson, C., Robertson, J. C., Rödel, R., Sindorf, N., and
503 Wisser, D.: High-resolution mapping of the world’s reservoirs and dams for sustainable river-
504 flow management, *Front. Ecol. Environ.*, 9, 494–502, <https://doi.org/10.1890/100125>, 2011.
- 505 Liu, J. and Yang, W.: Water sustainability for China and beyond, *Science (80-.)*, 337, 649–650,
506 <https://doi.org/10.1126/science.1219471>, 2012.
- 507 Ma, R. H., Yang, G. S., Duan, H. T., Jiang, J. H., Wang, S. M., Feng, X. Z., Li, A. N., Kong, F.
508 X., Xue, B., Wu, J. L., and Li, S. J.: China’s lakes at present: Number, area and spatial
509 distribution, *Sci. China Earth Sci.*, 54, 283–289, <https://doi.org/10.1007/s11430-010-4052-6>,
510 2011.
- 511 Mulligan, M., van Soesbergen, A., and Sáenz, L.: GOODD, a global dataset of more than 38,000
512 georeferenced dams, *Sci. Data*, 7, 1–8, <https://doi.org/10.1038/s41597-020-0362-5>, 2020.
- 513 Murray, N. J., Phinn, S. R., DeWitt, M., Ferrari, R., Johnston, R., Lyons, M. B., Clinton, N.,
514 Thau, D., and Fuller, R. A.: The global distribution and trajectory of tidal flats, *Nature*, 565, 222,
515 <https://doi.org/10.1038/s41586-018-0805-8>, 2019.
- 516 Ogilvie, A., Belaud, G., Massuel, S., Mulligan, M., Le Goulven, P., and Calvez, R.: Surface
517 water monitoring in small water bodies: Potential and limits of multi-sensor Landsat time series,
518 *Hydrol. Earth Syst. Sci.*, 22, 4349–4380, <https://doi.org/10.5194/hess-22-4349-2018>, 2018.



- 519 Paredes-Beltran, B., Sordo-Ward, A., and Garrote, L.: Dataset of Georeferenced Dams in South
520 America (DDSA), *Earth Syst. Sci. Data*, <https://doi.org/10.5194/essd-13-213-2021>, 2021.
- 521 Pekel, J. F., Cottam, A., Gorelick, N., and Belward, A. S.: High-resolution mapping of global
522 surface water and its long-term changes, *Nature*, 540, 418, <https://doi.org/10.1038/nature20584>,
523 2016.
- 524 Ran, L., Butman, D. E., Battin, T. J., Yang, X., Tian, M., Duvert, C., Hartmann, J., Geeraert, N.,
525 and Liu, S.: Substantial decrease in CO₂ emissions from Chinese inland waters due to global
526 change, *Nat. Commun.*, 12, 1–9, <https://doi.org/10.1038/s41467-021-21926-6>, 2021.
- 527 Slater, J. A., Garvey, G., Johnston, C., Haase, J., Heady, B., Kroenung, G., and Little, J. K.: The
528 SRTM Data Finishing Process and Products, *Photogramm. Eng. Remote Sensing*, 72, 237–247,
529 2006.
- 530 Tao, S., Zhang, H., Feng, Y., and Zhu, J.: Changes in China’s water resources in the early 21st
531 century, *Front. Ecol. Environ.*, <https://doi.org/10.1002/fee.2164>, 2020.
- 532 Thornton, J., Steel, A., and Rast, W.: Chapter 8* - Reservoirs, in: *Water quality assessments : a*
533 *guide to the use of biota, sediments and water in environmental monitoring*, 2–3, 1996.
- 534 Wang, J., Sheng, Y., Gleason, C. J., and Wada, Y.: Downstream Yangtze River levels impacted
535 by Three Gorges Dam, *Environ. Res. Lett.*, 8, 044012, [https://doi.org/10.1088/1748-](https://doi.org/10.1088/1748-9326/8/4/044012)
536 [9326/8/4/044012](https://doi.org/10.1088/1748-9326/8/4/044012), 2013.



- 537 Wang, J., Walter, B. A., Yao, F., Song, C., Ding, M., Maroof, A. S., Zhu, J., Fan, C., Xin, A.,
538 McAlister, J. M., Sikder, S., Sheng, Y., Allen, G. H., Crétaux, J.-F., and Wada, Y.: GeoDAR:
539 Georeferenced global dam and reservoir dataset for bridging attributes and geolocations, *Earth*
540 *Syst. Sci. Data*, 2021, 1–52, <https://doi.org/10.5194/essd-2021-58>, 2021a.
- 541 Wang, X., Xiao, X., Zou, Z., Dong, J., Qin, Y., Doughty, R. B., Menarguez, M. A., Chen, B.,
542 Wang, J., Ye, H., Ma, J., Zhong, Q., Zhao, B., and Li, B.: Gainers and losers of surface and
543 terrestrial water resources in China during 1989 – 2016, *Nat. Commun.*, 11, 1–12,
544 <https://doi.org/10.1038/s41467-020-17103-w>, 2020a.
- 545 Wang, X., Xiao, X., Zou, Z., Hou, L., Qin, Y., Dong, J., Doughty, R. B., Chen, B., Zhang, X.,
546 Chen, Y., Ma, J., Zhao, B., and Li, B.: Mapping coastal wetlands of China using time series
547 Landsat images in 2018 and Google Earth Engine, *ISPRS J. Photogramm. Remote Sens.*, 163,
548 312–326, <https://doi.org/10.1016/j.isprsjprs.2020.03.014>, 2020b.
- 549 Wang, X., Xiao, X., Xu, X., Zou, Z., Chen, B., Qin, Y., Zhang, X., Dong, J., Liu, D., Pan, L., and
550 Li, B.: Rebound in China’s coastal wetlands following conservation and restoration, *Nat.*
551 *Sustain.*, 4, 1076–1083, <https://doi.org/10.1038/s41893-021-00793-5>, 2021b.
- 552 Wu, J., Huang, J., Han, X., Gao, X., He, F., Jiang, M., Jiang, Z., Primack, R. B., and Shen, Z.:
553 The Three Gorges Dam: An ecological perspective, *Front. Ecol. Environ.*, 2, 241–248,
554 [https://doi.org/10.1890/1540-9295\(2004\)002\[0241:TTGDAE\]2.0.CO;2](https://doi.org/10.1890/1540-9295(2004)002[0241:TTGDAE]2.0.CO;2), 2004.
- 555 Wulder, M. A., White, J. C., Loveland, T. R., Woodcock, C. E., Belward, A. S., Cohen, W. B.,



- 556 Fosnight, E. A., Shaw, J., Masek, J. G., and Roy, D. P.: The global Landsat archive: Status,
557 consolidation, and direction, *Remote Sens. Environ.*, 185, 271–283,
558 <https://doi.org/10.1016/j.rse.2015.11.032>, 2016.
- 559 Xiang, Y., Fu, Z., Meng, Y., Zhang, K., and Cheng, Z.: Analysis of wave clipping effects of
560 plain reservoir artificial islands based on MIKE21 SW model, *Water Sci. Eng.*, 12, 179–187,
561 <https://doi.org/https://doi.org/10.1016/j.wse.2019.08.002>, 2019.
- 562 Yang, X. and Lu, X.: Drastic change in China’s lakes and reservoirs over the past decades, *Sci.*
563 *Rep.*, 4, 6041, <https://doi.org/10.1038/srep06041>, 2014.
- 564 Yang, X. and Lu, X. X.: Delineation of lakes and reservoirs in large river basins: An example of
565 the Yangtze River Basin, China, <https://doi.org/10.1016/j.geomorph.2013.02.018>, 2013.
- 566 Zhang, Q., Li, L., Wang, Y. G., Werner, A. D., Xin, P., Jiang, T., and Barry, D. A.: Has the
567 Three-Gorges Dam made the Poyang Lake wetlands wetter and drier?, *Geophys. Res. Lett.*, 39,
568 L20402, <https://doi.org/10.1029/2012GL053431>, 2012.
- 569 Zhou, F., Bo, Y., Ciais, P., Dumas, P., Tang, Q., Wang, X., Liu, J., Zheng, C., Polcher, J., Yin,
570 Z., Guimberteau, M., Peng, S., Otle, C., Zhao, X., Zhao, J., Tan, Q., Chen, L., Shen, H., Yang,
571 H., Piao, S., Wang, H., and Wada, Y.: Deceleration of China’s human water use and its key
572 drivers, *Proc. Natl. Acad. Sci. U. S. A.*, 117, 7702–7711,
573 <https://doi.org/10.1073/pnas.1909902117>, 2020.
- 574 Zhou, Y., Dong, J., Xiao, X., Xiao, T., Yang, Z., Zhao, G., Zou, Z., and Qin, Y.: Open surface



575 water mapping algorithms: A comparison of water-related spectral indices and sensors, 9, 256,
576 <https://doi.org/10.3390/w9040256>, 2017.

577 Zhou, Y., Dong, J., Liu, J., Metternicht, G., Shen, W., You, N., Zhao, G., and Xiao, X.: Are there
578 sufficient Landsat observations for retrospective and continuous monitoring of land cover
579 changes in China?, *Remote Sens.*, 11, <https://doi.org/10.3390/rs11151808>, 2019a.

580 Zhou, Y., Dong, J., Xiao, X., Liu, R., Zou, Z., Zhao, G., and Ge, Q.: Continuous monitoring of
581 lake dynamics on the Mongolian Plateau using all available Landsat imagery and Google Earth
582 Engine, *Sci. Total Environ.*, 689, 366–380, <https://doi.org/10.1016/J.SCITOTENV.2019.06.341>,
583 2019b.

584 Zhu, Z., Wang, S., and Woodcock, C. E.: Improvement and expansion of the Fmask algorithm:
585 Cloud, cloud shadow, and snow detection for Landsats 4-7, 8, and Sentinel 2 images, *Remote*
586 *Sens. Environ.*, 159, 269–277, <https://doi.org/10.1016/j.rse.2014.12.014>, 2015.

587 Zou, Z. H., Dong, J. W., Menarguez, M. A., Xiao, X. M., Qin, Y. W., Doughty, R. B., Hooker,
588 K. V, and Hambright, K. D.: Continued decrease of open surface water body area in Oklahoma
589 during 1984-2015, *Sci. Total Environ.*, 595, 451–460,
590 <https://doi.org/10.1016/j.scitotenv.2017.03.259>, 2017.

591 Zou, Z. H., Xiao, X. M., Dong, J. W., Qin, Y. W., Doughty, R. B., Menarguez, M. A., Zhang, G.
592 L., and Wang, J.: Divergent trends of open-surface water body area in the contiguous United
593 States from 1984 to 2016, *Proc. Natl. Acad. Sci. U. S. A.*, 115, 3810–3815,



594 <https://doi.org/10.1073/pnas.1719275115>, 2018.

595

596

597

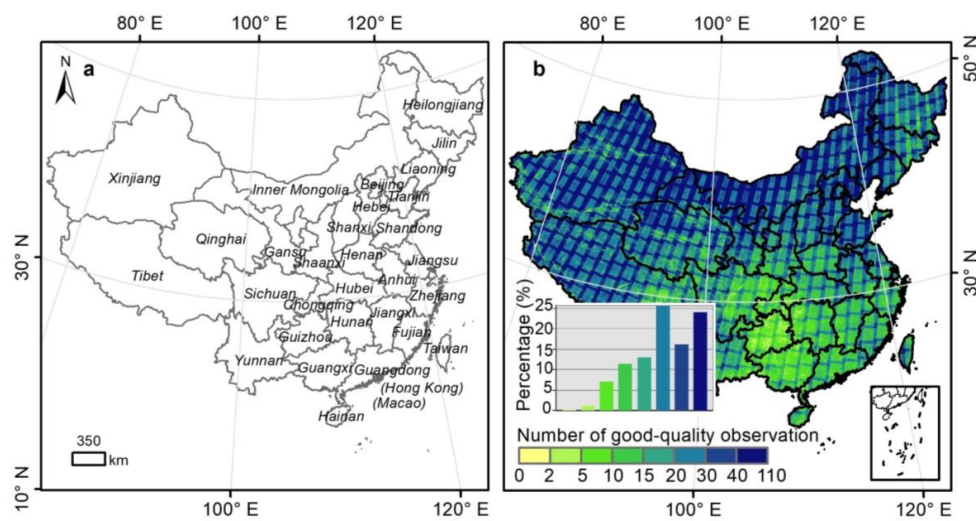
598 **Figures and figure legends**



599

600 **Fig. 1.** Types of reservoirs in China within high-resolution images (© Google Earth Pro 2019). (a-

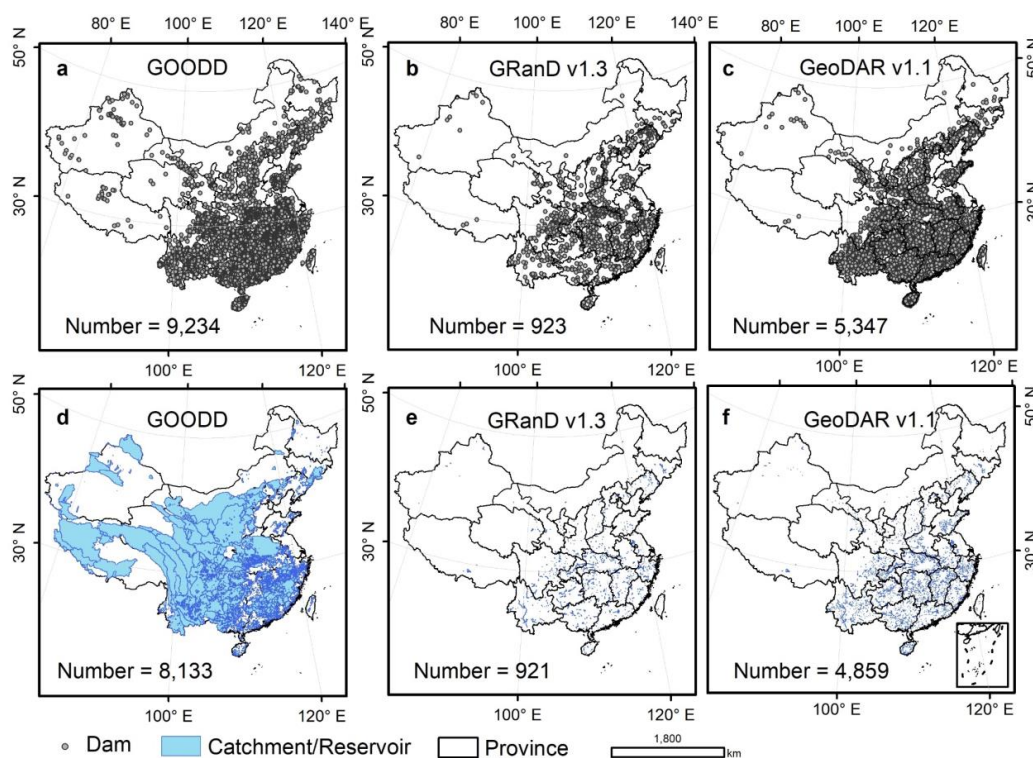
601 b) Impoundment reservoir; (c-d) Mountain reservoir; (e-f) Plain reservoir.



602

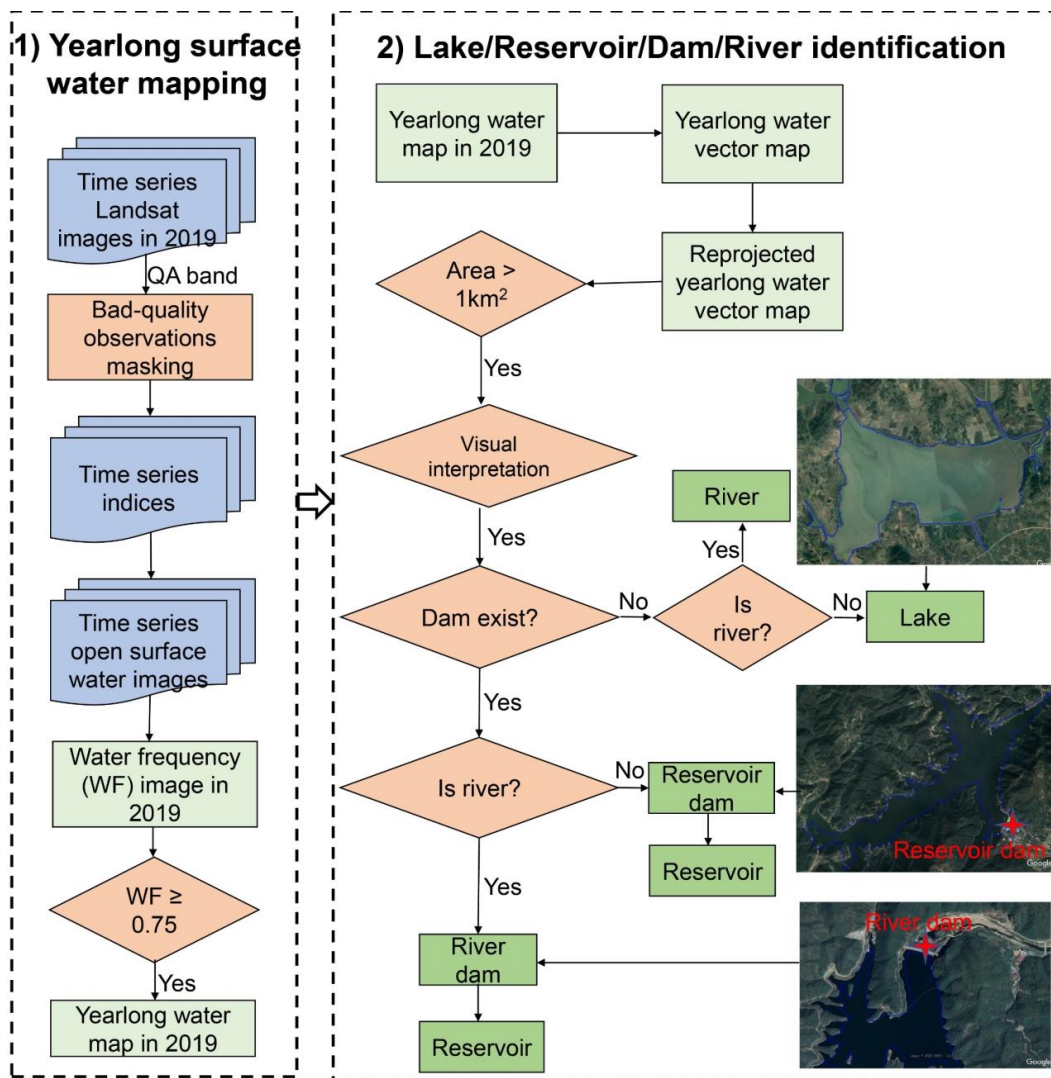
603 **Fig. 2.** Spatial distribution of provinces (a) and numbers of Landsat good-quality observations (b)

604 in China for 2019.



605

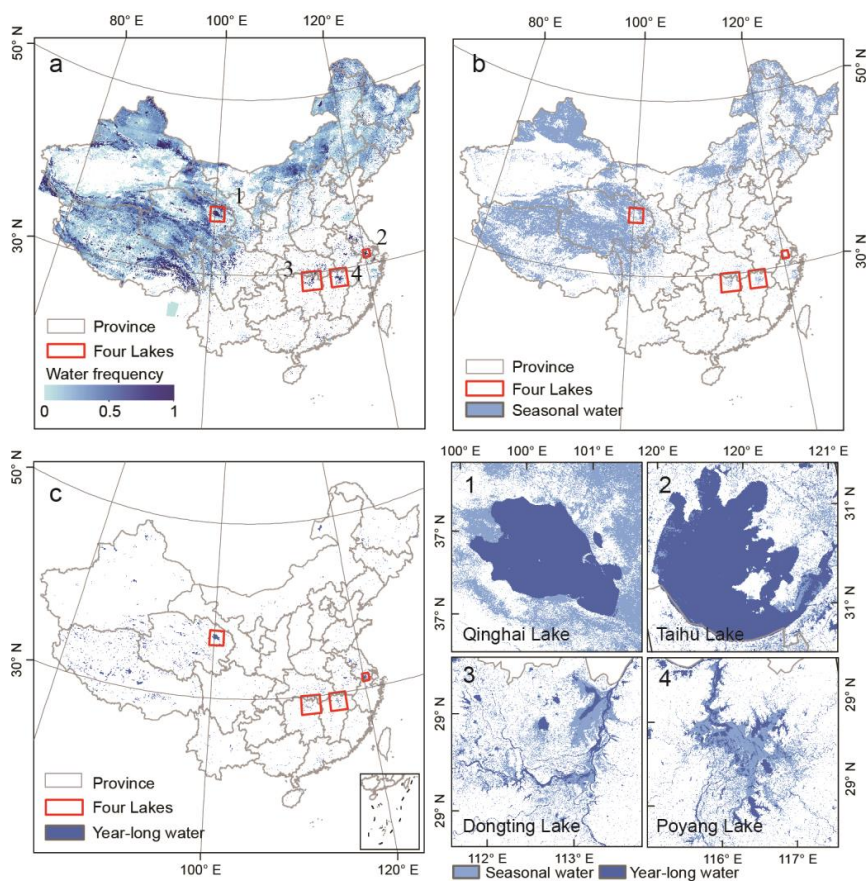
606 **Fig. 3.** Spatial distribution of dams from the GLObal GeOreferenced Database of Dams (GOODD)
607 (a) (Mulligan et al., 2020), the Global Reservoir and Dam (GRanD) v1.3 (b) (Lehner et al., 2011),
608 and the Georeferenced global Dam And Reservoir (GeoDAR) v1.1 (c) (Wang et al., 2021) datasets.
609 The GOODD dataset reported the catchment of each dam (d) while the GRanD and GeoDAR
610 datasets reported the reservoir information of each dam (e, f).



611

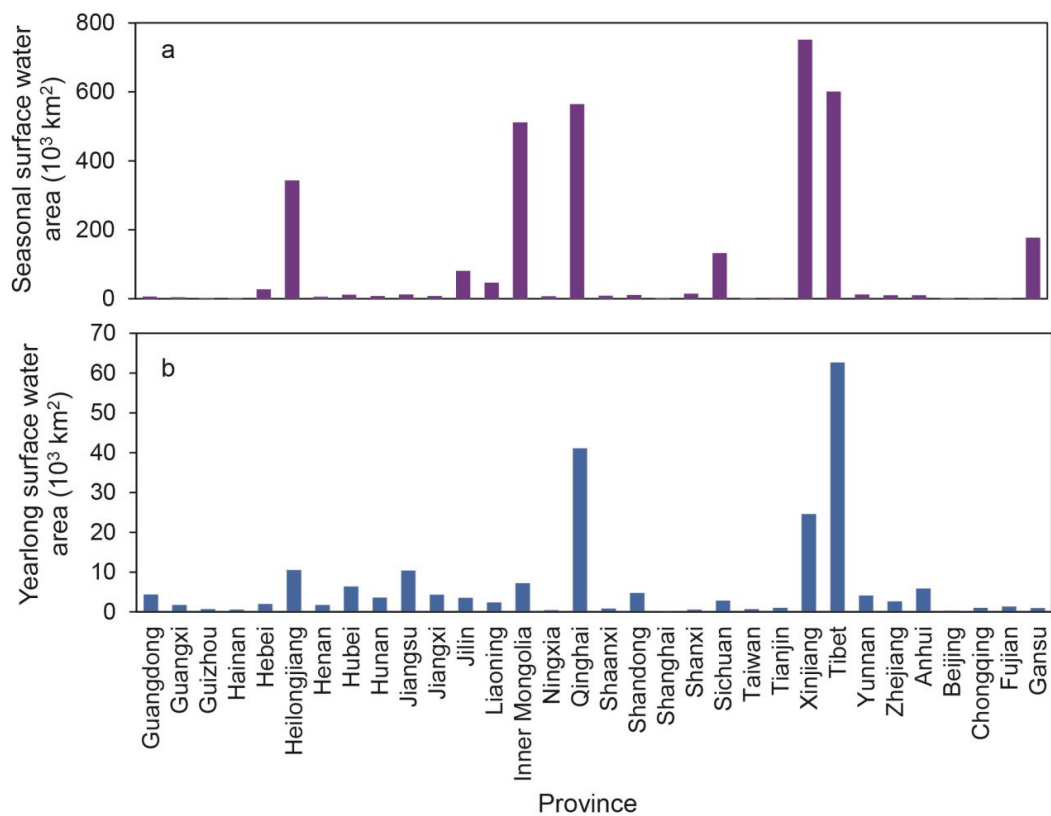
612 **Fig. 4.** Schematic flowchart of lakes, reservoirs, dams, and rivers identification in this study. The

613 images were acquired from Google Earth Pro (© Google Earth Pro 2019).



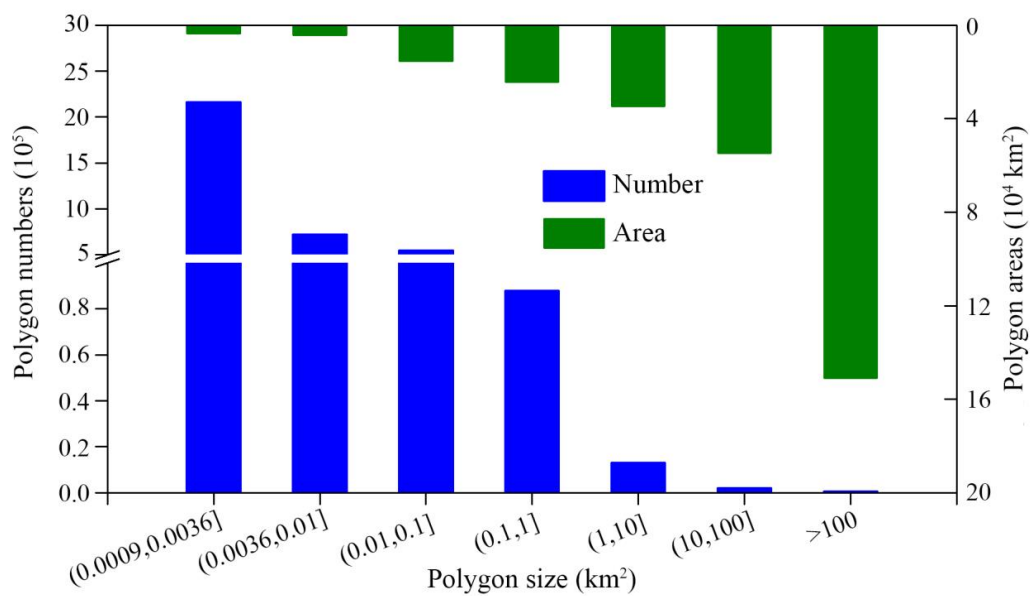
614

615 **Fig. 5.** Spatial distribution of surface water body (SWB) in China for 2019. (a), Water frequency,
616 (b), Seasonal SWB, (c), Yearlong SWB. Subfigures (1-4) are three zoom-in views of seasonal and
617 year-long SWB in Qinghai Lake, Taihu Lake, Dongting Lake, and Poyang Lake in China.



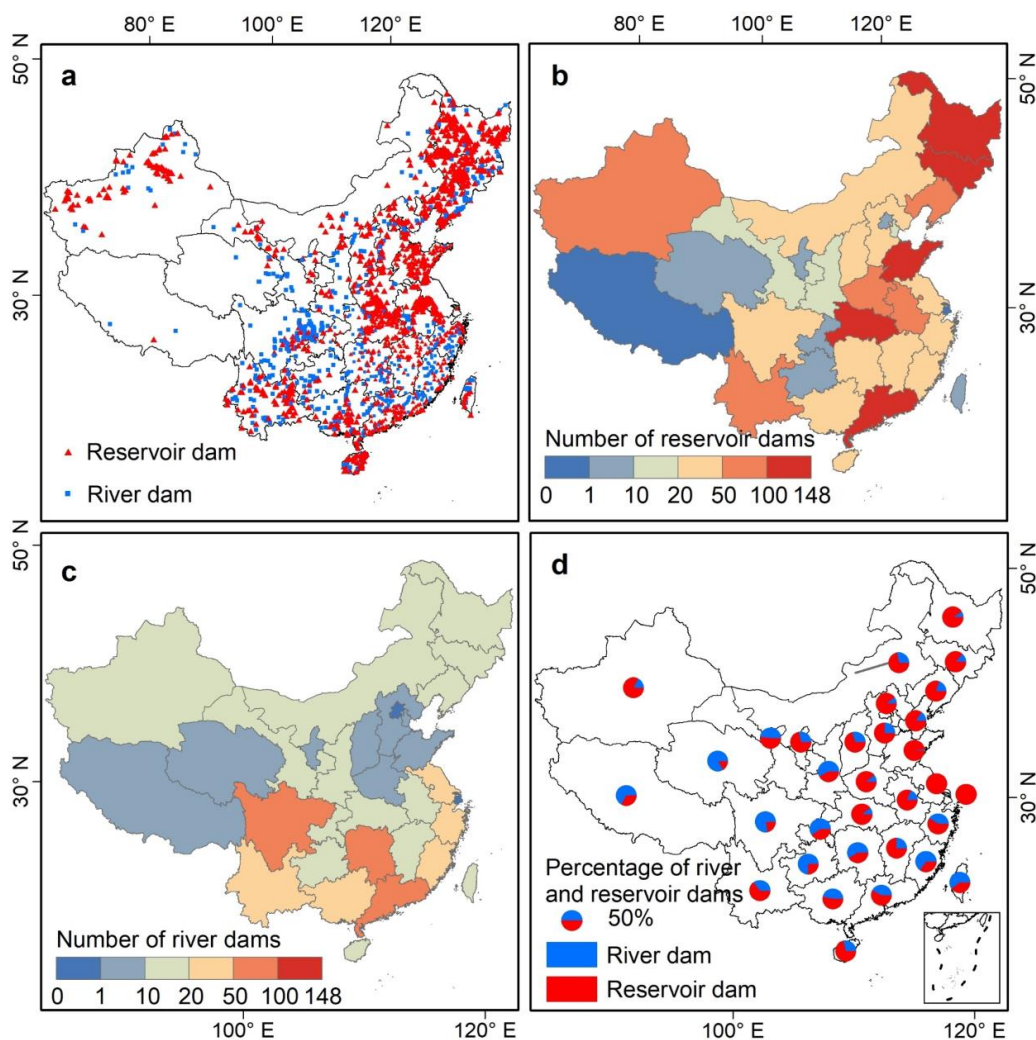
618

619 **Fig. 6.** Areas of seasonal (a) and yearlong (b) surface water bodies by province in China for 2019.



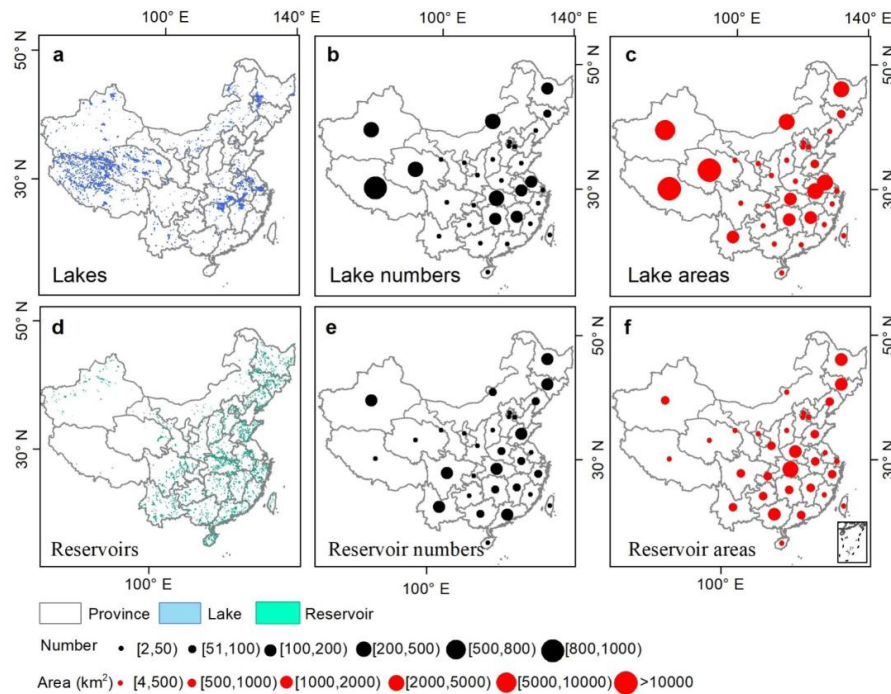
620

621 **Fig. 7.** Numbers and areas of yearlong surface water body polygons with different sizes.



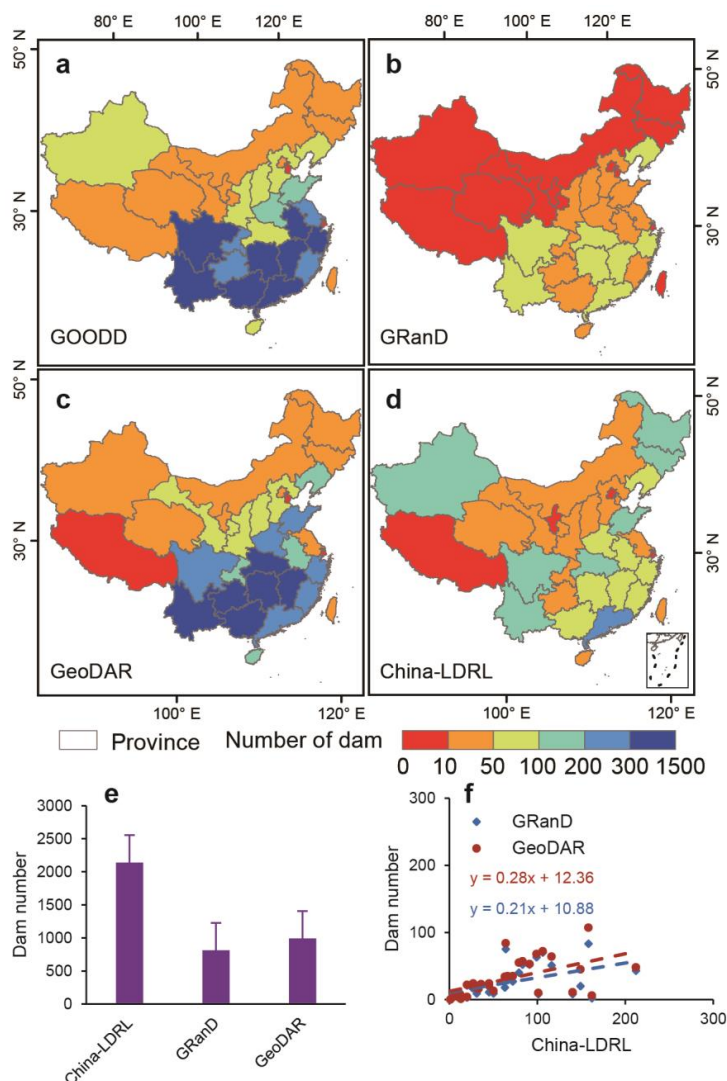
622

623 **Fig. 8.** Distribution of river dams and reservoir dams in China for 2019. **a**, Spatial distribution of
624 river dams and reservoir dams; **b**, Number of reservoir dams by province; **c**, Number of river dams
625 by province; **d**, Percentage of river dams and reservoir dams by province.



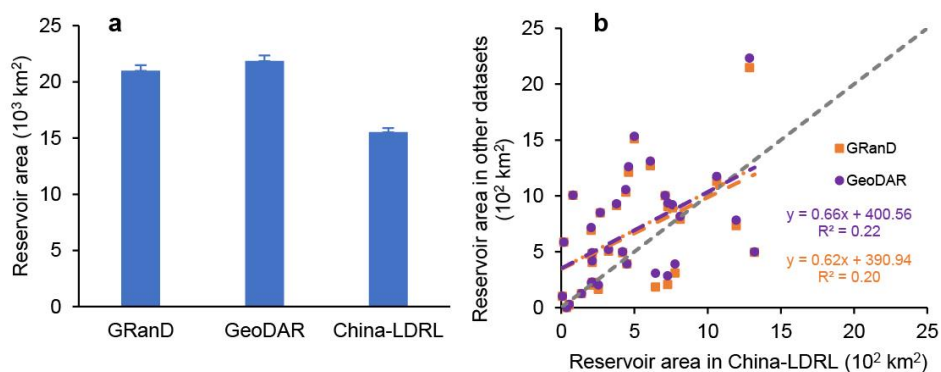
626

627 **Fig. 9.** Distribution of lakes and reservoirs in China. **a**, Spatial distribution of lakes; **b**, Lake
628 numbers by province; **c**, Lake areas by province; **d**, Spatial distribution of reservoirs; **e**, Reservoir
629 numbers by province; **f**, Reservoir areas by province.



630

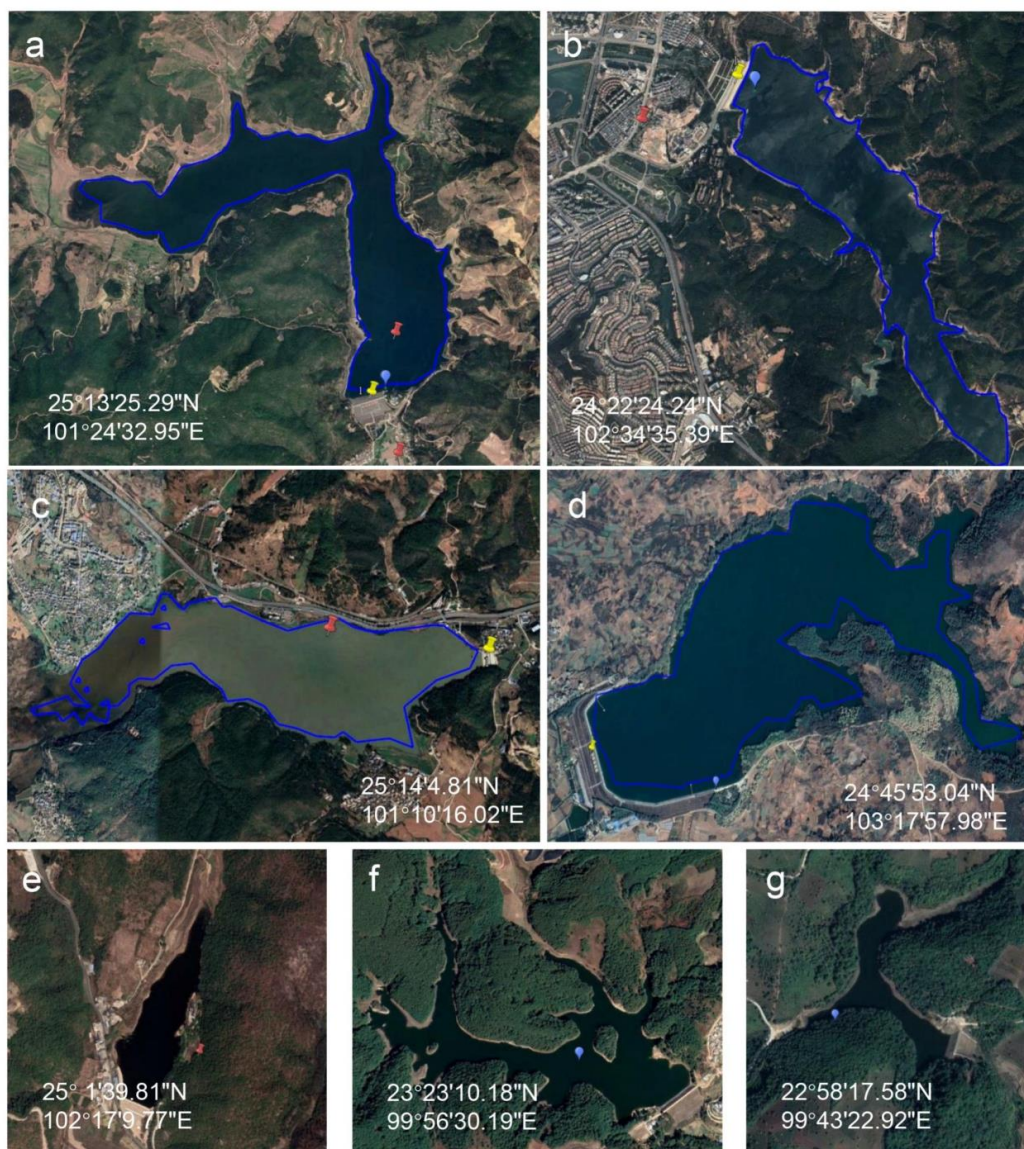
631 **Fig. 10.** Numbers of large dams of different datasets. (a) Dam number in the GOODD dataset by
 632 province; (b) Dam number in the GRanD dataset by province; (c) Dam number in the GeoDAR
 633 dataset by province; (d) Dam number in the China-LDRL dataset by province; (e) Large dam
 634 numbers of different datasets in China; (f) The relationships of large dam numbers between China-
 635 LDRL and GRand and GeoDAR datasets.



636

637 **Fig. 11.** Areas of large reservoir (a) and their relationships (b) of the GRanD, GeoDAR, and our

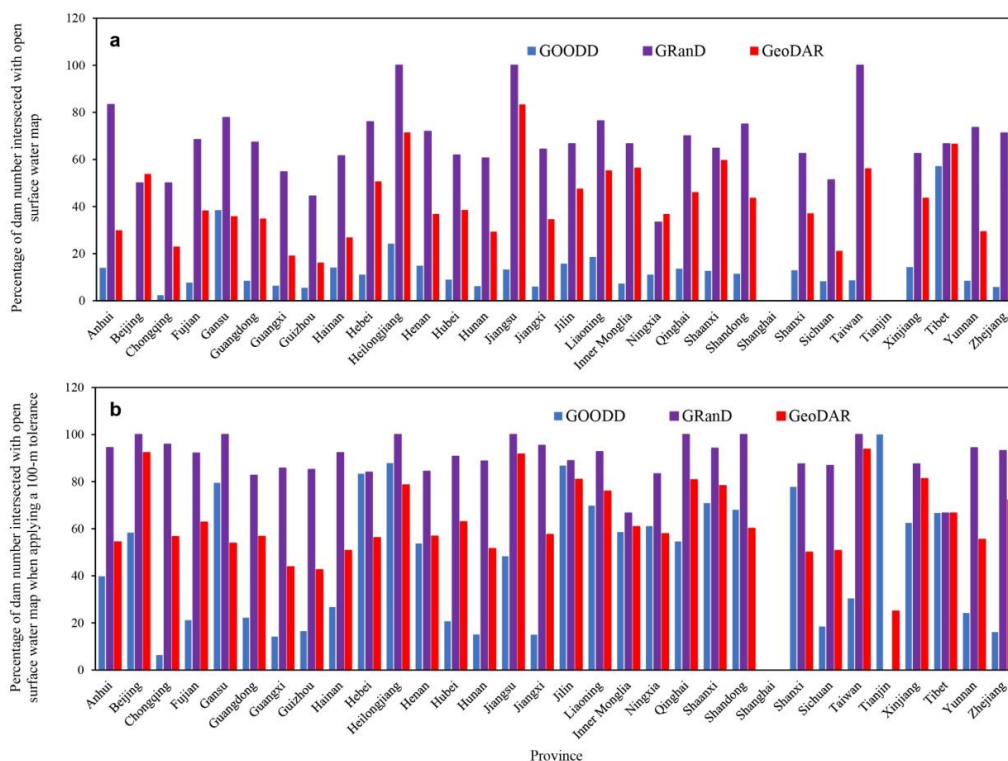
638 China-LDRL datasets.



639

640 **Fig. 12.** Dam from the GOODD, GeoDAR, and China-LDRL datasets within Google Earth Pro (©

641 Google Earth Pro 2019).



642

643 **Fig. 13.** The numbers of dams intersected with surface water body (SWB) map in China for 2019

644 by province. (a) Percentage of numbers of dams intersected with SWB map; (b) Percentage of

645 numbers of dams intersected with SWB map when applying a 100-m tolerance.